1 **Ultrapotent SARS-CoV-2 neutralizing antibodies with protective efficacy against**

2 **newly emerged mutational variants**

3 Tingting Li[1,2,*], Xiaojian Han[1,2,*], Chenjian Gu[3,*], Hangtian Guo[4,5,*], Huajun Zhang[6,*],

4 Yingming Wang[1,2,*], Chao Hu[1,2], Kai Wang[7], Fengjiang Liu[4], Feiyang Luo[1,2], Yanan

5 Zhang[8,9], Jie Hu[7], Wang Wang[1,2], Shenglong Li[1,2], Yanan Hao[1,2], Meiying Shen[10],

6 Jingjing Huang[1,2], Yingyi Long[1,2], Shuyi Song[1,2], Ruixin Wu[1,2], Song Mu[1,2], Qian

7 Chen[1,2], Fengxia Gao[1,2], Jianwei Wang[1,2], Shunhua Long[1,2], Luo Li[1,2], Yang Wu[3], Yan

8 Gao[4], Wei Xu[3], Xia Cai[3], Di Qu[3], Zherui Zhang[8,9], Hongqing Zhang[8,9], Na Li[8,9],

9 Qingzhu Gao[7], Guiji Zhang[7], Changlong He[7], Wei Wang[11], Xiaoyun Ji[5,11], Ni Tang[7],

10 Zhenghong Yuan[3], Youhua Xie[3,†], Haitao Yang[4,†], Bo Zhang[8,†], Ailong Huang[7,†] and

11 Aishun Jin[1,2,†]

12 [1]Department of Immunology, College of Basic Medicine, Chongqing Medical

13 University, Chongqing, 400010, China

14 [2]Chongqing Key Laboratory of Basic and Translational Research of Tumor

15 Immunology, Chongqing Medical University, Chongqing, 400010, China

16 [3]Key Laboratory of Medical Molecular Virology, Department of Medical

17 Microbiology and Parasitology, School of Basic Medical Sciences, Shanghai Medical

18 College, Fudan University, Shanghai, 200032, China

19 [4]Shanghai Institute for Advanced Immunochemical Studies and School of Life

20 Science and Technology, ShanghaiTech University, Shanghai, 201210, China

21 [5]State Key Laboratory of Pharmaceutical Biotechnology, School of Life Sciences,

22 Nanjing University, Nanjing, Jiangsu, 210023, China

23   [6]State Key Laboratory of Virology, Wuhan Institute of Virology, Center for Biosafety

24   Mega-Science, Chinese Academy of Sciences, Wuhan, 430071, China

25   [7]Key Laboratory of Molecular Biology on Infectious Diseases, Ministry of Education,

26   Chongqing Medical University, Chongqing, 400010, China

27   [8]Key Laboratory of Special Pathogens and Biosafety, Wuhan Institute of Virology,

28   Center for Biosafety Mega-Science, Chinese Academy of Sciences, Wuhan, 430071,

29   China

30   [9]University of Chinese Academy of Sciences, Beijing, 100049, China

31   [10]Department of Breast Surgery, Harbin Medical University Cancer Hospital, Harbin,

32   150000, China

33   [11]Institute of life sciences, Chongqing Medical University, Chongqing, 400010, China

34   [*]These authors contributed equally.

35

36   [†]Correspondence: yhxie@fudan.edu.cn (Y.H.X); yanght@shanghaitech.edu.cn

37   (H.T.Y); zhangbo@wh.iov.cn (B.Z); ahuang@cqmu.edu.cn (A.L.H);

38   aishunjin@cqmu.edu.cn (A.S.J)

39

40

41   **Abstract**

42   Accumulating mutations in the SARS-CoV-2 Spike (S) protein can increase the

43   possibility of immune escape, challenging the present COVID-19 prophylaxis and

44   clinical interventions. Here, 3 receptor binding domain (RBD) specific monoclonal

45   antibodies (mAbs), 58G6, 510A5 and 13G9, with high neutralizing potency blocking

46   authentic SARS-CoV-2 virus displayed remarkable efficacy against authentic B.1.351

47   virus. Each of these 3 mAbs in combination with one neutralizing Ab recognizing

48   non-competing epitope exhibited synergistic effect against authentic SARS-CoV-2

49   virus. Surprisingly, structural analysis revealed that 58G6 and 13G9, encoded by the

50   *IGHV1-58* and the *IGKV3-20* germline genes, both recognized the steric region

51    $S^{470-495}$ on the RBD, overlapping the E484K mutation presented in B.1.351. Also,

52   58G6 directly bound to another region $S^{450-458}$ in the RBD. Significantly, 58G6 and

53   510A5 both demonstrated prophylactic efficacy against authentic SARS-CoV-2 and

54   B.1.351 viruses in the transgenic mice expressing human ACE2 (hACE2), protecting

55   weight loss and reducing virus loads. These 2 ultrapotent neutralizing Abs can be

56   promising candidates to fulfill the urgent needs for the prolonged COVID-19

57   pandemic.

58

59 **Introduction**

60 The persistence of COVID-19 in the global population can result in the accumulation

61 of specific mutations of SARS-CoV-2 with increased infectivity and/or reduced

62 susceptibility to neutralization[1-12]. Highly transmissible SARS-CoV-2 variants, such

63 as B.1.351 emerged in South Africa, harbor multiple immune escape mutations, and

64 have raised global concerns for the efficacy of available interventions and for

65 re-infection[2-9,11]. As these challenges presented, the protective efficacy of current

66 antibody-based countermeasures needs to be thoroughly assessed against the current

67 mutational variants.

68 The major interest of neutralizing therapies has been targeted towards SARS-CoV-2

69 RBD, which is the core region for the host cell receptor ACE2 engagement[13-23].

70 B.1.351 bears 3 mutations, S^{K417N}, S^{E484K} and S^{N501Y}, in its RBD, the first 2 of which

71 have been proven to be the cause for its evasion from neutralizing Ab and serum

72 responses[2-9]. Nevertheless, a small group of SARS-CoV-2 RBD specific neutralizing

73 Abs demonstrated undisturbed *in vitro* potency against B.1.351[2,4-7,9]. Evaluating their

74 therapeutic efficacy against the circulating strains is necessary for the reformulation of

75 protective interventions and vaccines against the evolving pandemic.

76 Here, we focused on 20 neutralizing Abs selected from a SARS-CoV-2 RBD

77 specific mAb reservoir and confirmed their potency against authentic SARS-CoV-2

78 virus. Excitingly, at least 3 of our mAbs showed remarkable neutralizing efficacy

79 against authentic B.1.351 virus. 58G6, one of our top neutralizing Abs, was found to

4

80   target a region of $S^{450-458}$ and a steric site $S^{470-495}$ on the receptor binding motif (RBM).

81   Furthermore, ultrapotent 58G6 and 510A5 exhibited strong prophylactic efficacy in

82   SARS-CoV-2- and B.1.351-infected hACE2-transgenic mice. Our study has

83   characterized a pair of neutralizing Abs with potential effective therapeutic value in

84   clinical applications, which may provide updated information for RBD specific mAbs

85   against the prolonged COVID-19 pandemic.

86

87   **Results**

88   **SARS-CoV-2 RBD specific neutralizing Abs exhibited sustained efficacy against**

89   **authentic B.1.351**

90   By our recently established rapid neutralizing Abs screening system[24], we have

91   successfully obtained 20 neutralizing Abs with high affinities to SARS-CoV-2 RBD

92   from COVID-19 convalescent individuals, and their neutralizing potencies were

93   confirmed by the half inhibition concentrations (IC_{50}s) against authentic SARS-CoV-2

94   virus quantified via qRT-PCR (Fig. 1a, c and Extended Data Fig. 1). Here, we

95   analyzed the neutralizing potency of our top 10 neutralizing Abs against authentic

96   SARS-CoV-2 and B.1.351 viruses by the plaque-reduction neutralization testing

97   (PRNT). At least 3 of our potent neutralizing Abs 58G6, 510A5 and 13G9 exhibited

98   striking neutralizing efficacy against SARS-CoV-2, with the IC_{50}s value ranging from

99   1.285 to 9.174 ng/mL (Fig. 1b, c). Importantly, the RBD escape mutations of B.1.351

100 did not compromise the neutralizing efficacy of 58G6 and 510A5, with the IC_{50}s of

101 1.660 and 2.235 ng/ml respectively (Fig. 1b, c). As reported for a wide range of RBD

102 specific neutralizing Abs[2-9], authentic B.1.351 virus has challenged some of the tested

103 mAbs (Fig. 1b, c). However, majority of our top 10 mAbs still exhibited neutralizing

104 capabilities against this variant (Fig. 1b, c). Of note, the neutralizing potencies of all

105 10 mAbs against the B.1.1.7 pseudovirus were shown to be similar to those against

106 the SARS-CoV-2 pseudovirus (Fig. 1c and Extended Data Fig. 2). In addition, the

107 binding affinity of 58G6 to the B.1.351 S1 subunit was comparable to that to the

108 SARS-CoV-2 S1, while 510A5 and 13G9 showed higher binding affinity to the S1

109 subunit of SARS-CoV-2 than that of B.1.351 (Extended Data Fig. 3). Majority of

110 these top 20 neutralizing Abs exhibited no cross-reactivity to the SARS-CoV S

111 protein or the MARS-CoV S protein (Extended Data Fig. 4). Collectively, 3 RBD

112 specific mAbs demonstrated potent neutralizing efficacy against authentic

113 SARS-CoV-2 and B.1.351 viruses, suggesting that our neutralizing Abs might be

114 applied for the current COVID-19 pandemic.

115

116 **The epitopes for potent neutralizing Abs overlapped a key site on SARS-CoV-2**

117 **RBD**

118 To define potential antigenic sites on SARS-CoV-2 RBD, we performed competitive

119 ELISA with the above top 20 neutralizing Abs and the other 54 mAbs selected from

120 our developed RBD-specific mAb reservoir. As shown in Fig. 2a, 5 groups of mAbs

121   were identified according to their recognition sites, each of which consisted of mAbs

122   competing for the epitope for 13G9 (13G9e), the epitope recognized by a

123   non-neutralizing SARS-CoV-2 specific mAb 81A11 (81A11e), or the epitope

124   recognized by a SARS-CoV specific neutralizing Ab CR3022 (CR3022e) (Fig. 2a).

125   Interestingly, the epitopes recognized by the majority of potent neutralizing Abs

126   overlapped with 13G9e (Fig. 2a). Next, we confirmed that the top 20 mAbs could

127   directly inhibit the interaction of SARS-CoV-2 RBD and ACE2 by the competitive

128   ELISA and surface plasmon resonance (SPR) assay (Extended Data Fig. 5 and 6). To

129   assess the interrelationships between the epitopes recognized by our top 20

130   neutralizing Abs in detail, we performed competitive ELISA using biotinylated mAbs.

131   We found that 16 of them competed with 13G9, whereas the antigenic sites of the

132   other 4 Abs (510A5, 55A8, 57F7 and 07C1) overlapped with an independent epitope

133   (510A5e) (Extended Data Fig. 7). These findings suggest that there are at least 2

134   independent epitopes on the RBD related to SARS-CoV-2 neutralization, from which

135   13G9e may represent a key antigenic site for the binding of potent neutralizing Abs to

136   the RBD.

137   To test whether our mAbs could elicit synergistic effect against SARS-CoV-2, we

138   paired each of the top 3 neutralizing Abs (58G6, 510A5 or 13G9) with one Ab

139   exhibiting much lower potency from another group shown in Fig 2a. Synergistic

140   effects were observed for all combinations at higher levels of inhibition against the

141   authentic virus, confirming the synergistic advantage of neutralizing Ab cocktails (Fig.

142   2b-d). Of note, adding neutralizing Ab from a different cluster barely reduced the

7

143 IC$_{50}$s of the top 3 mAbs, indicating that our potent mAbs alone were sufficient in

144 neutralizing SARS-CoV-2 (Fig. 2b-d).

145

58G6 recognized a linear binding region in the denatured RBD

147 To determine the precise interactive regions of our potent neutralizing Abs, first, we

148 assessed the binding ability of the top 20 mAbs to the denatured RBD. In a

149 preliminary screening, 9 mAbs from our top 20 mAbs to SARS-CoV-2 RBD were

150 found to be capable of directly binding to the denatured RBD (Extended Data Fig. 8).

151 Therefore, we designed and synthesized fifteen 20-mer peptides (RBD1 to RBD15),

152 overlapping with 5 amino acids, to cover the entire sequence of the RBD, as amino

153 acids 319-541 of SARS-CoV-2 S (S$^{319-541}$) (Extended Data Fig. 9a). Unexpectedly,

154 instead of a continuous linear region, we found that 5 of these 9 mAbs could

155 simultaneously recognize 3 independent fragments (RBD2, RBD9 and RBD13), while

156 58G6 only strongly bound to RBD9 (S$^{439-459}$) (Extended Data Fig. 9b, c). To

157 determine the essential amino acid residues in the RBD accounted for 58G6 binding,

158 we re-synthesized two 20-mer peptides overlapping with 15 amino acids (RBD9-1

159 and RBD9-2), covering the RBD9 specific residues (Extended Data Fig. 9a). The

160 results of peptide ELISA revealed that 58G6 preferentially interacted with RBD9-1

161 than RBD9, in a dose-dependent manner, whereas no interaction of 58G6 with

162 RBD9-2 was observed (Fig. 3a, b). When we individually replaced each amino acid

163 residue in RBD9-1 (S$^{444-463}$) with alanine (A), we found that the binding of 58G6 to a

8

164 fragment of 8 amino acids ($S^{450-457}$) was significantly reduced (Fig. 3a). To a lesser

165 extent, $S^{445-449}$ and $S^{458-463}$ also slightly affected the binding of 58G6, and the former

166 might explain for the abolished interaction of 58G6 with RBD9-2 (Fig. 3a). Moreover,

167 we found that RBD9-1 bound to ACE2 in a dose-dependent manner, which could be

168 competitively inhibited by 58G6 (Fig. 3c-e). And the region of $S^{445-463}$ was identified

169 to be critical for the RBD9-1-ACE2 interaction (Fig. 3c, d). Hence, $S^{445-463}$ represents

170 an important region of SARS-CoV-2 RBD for the recognition of neutralizing Abs

171 represented by 58G6. It is worth mentioning that the interaction of 510A5 or 13G9

172 with the denatured RBD was not observed (Extended Data Fig. 8). Taken together, we

173 evidenced a linear region in the denatured RBD ($S^{450-457}$) that could be recognized by

174 58G6, which was one of the ultrapotent neutralizing Abs against authentic

175 SARS-CoV-2 and B.1.351 viruses.

176

177 **58G6 and 13G9 encoded by the *IGHV1-58* and *IGKV3-20* germline genes both**

178 **recognized the steric region of $S^{470-495}$ on the RBD**

179 To further investigate the molecular mechanism of our neutralizing Abs against

180 SARS-CoV-2, we determined the single-particle cryo-electron microscopy (cryo-EM)

181 structures of the antigen binding fragments (Fabs) of 58G6 or 13G9 in complex with

182 the modified SARS-CoV-2 S trimer with stabilizing mutations[25] (Extended Data Fig.

183 10a, b). We refined these two complex structures to the overall resolution of 3.6 Å for

184 58G6 and 3.9 Å for 13G9, respectively (Fig. 4a, b, Extended Data Fig. 10c-j and

9

185 Extended Data Table. 1). For either the 58G6 or the 13G9 complex, the

186 three-dimensional classification of the cryo-EM data showed the presence of a

187 dominant conformational state of S trimers in complex with the Fabs, with the

188 majority of selected particle images representing a 3-Fab-per-trimer complex (Fig. 4a,

189 b). As shown in Fig. 4a, in individual complex, each 58G6 Fab interacted with one

190 RBD in the "up" state. Similar to the structure of the 58G6 Fab-S complex, only one

191 dominant particle class was observed for the 13G9 Fab-S complex, corresponding to a

192 3-Fab-bound complex with all 3 RBDs in the "up" conformation (Fig. 4b).

193 Further refinement of the variable domains of 58G6 or 13G9 and the RBD to 3.5 Å

194 or 3.8 Å, respectively, revealed detailed molecular interactions within their binding

195 interface (Extended Data Fig. 10c-f, g-j). These two refined density maps along with

196 the predicted structures of the 58G6 and 13G9 Fabs were used to build the models to

197 illustrate detailed amino acid structures in three dimensions (Extended Data Fig. 11)[26].

198 Superimposition of the RBDs in the structures of 58G6 Fab-RBD and ACE2-RBD

199 complexes indicates a steric clash between ACE2 and the variable domains on the

200 heavy chain (HC) and the light chain (LC) of 58G6 Fab (Fig. 4c). Such observations

201 indicate that 58G6 can competitively inhibit the interaction between the SARS-CoV-2

202 RBD and ACE2. Likewise, an almost identical steric clash between 13G9 Fab and

203 ACE2 was observed, indicating that the SARS-CoV-2 RBD-ACE2 interaction can be

204 prohibited by 13G9 (Fig. 4c). When we compared the details of binding interface of

205 these 2 mAbs and RBD, they showed high level of structural similarity (Fig. 4d).

206 Specifically, majority of the complementarity determining regions (CDRs; CDRH2,

10

207 CDRH3, CDRL1 and CDRL3) of 58G6 Fab directly participate in the interaction with

208 the steric region of $S^{470-495}$ (Fig. 5a). Meanwhile, 13G9 Fab was shown to recognize

209 the same steric region using its CDRs: CDRH2, CDRH3, CDRL1 and CDRL3 (Fig.

210 5b). In parallel, an additional site of residues 450-458 on SARS-CoV-2 S ($S^{450-458}$)

211 was observed for 58G6 recognition (Fig. 5b), which contained the linear region of

212 $S^{450-457}$ we had identified with the denatured RBD, as shown above (Fig. 3a, b).

213   We found that both 58G6 and 13G9 were derived from *IGHV1-58* for the heavy

214 chain and *IGKV3-20* for the light chain, with a few differences in amino acid

215 constitution of their CDRH1, CDRH3 and CDRL3 (Extended Data Table. 2). These

216 identical germline gene origins correlated with the structural similarity between 58G6

217 and 13G9 (Fig. 4d). Several potential hydrogen bonds were identified on the contact

218 surface of each mAb and RBD, representing the unique network associated with

219 individual CDRs and amino acid residues within the epitope corresponding to each

220 mAb (Fig. 5c, d). In summary, these Fab-S complex structures suggest that 58G6 and

221 13G9 adopt the same potential neutralizing mechanism, wherein they are capable to

222 simultaneously bind to 3 RBDs, occluding the access of SARS-CoV-2 S to ACE2.

223 Notably, N94 in the CDRL3 of 58G6 or R94 in 13G9 forms a hydrogen bond with the

224 carbonyl group on the main chain, rather than the side chain, of S^{E484} (Fig. 5c, d).

225 Moreover, direct contact with a hydrogen bond was found between T105 in the

226 CDRH3 of 58G6 and K458 in the RBD, but not for S105 in 13G9 (Fig. 5c, d).

227

228 **58G6 and 510A5 showed protective efficacy against SARS-CoV-2 and B.1.351 *in***

229 ***vivo***

230 Given the IC_{50}s of our mAbs 58G6 and 510A5 against authentic B.1.351 were as low

231 as approximately 2 ng/mL *in vitro*, we tested their prophylactic efficacy in the

232 transgenic animal model. Different groups of hACE2 mice received intraperitoneal

233 administration of these 2 mAbs or PBS 24 hours before an intranasal challenge with

234 authentic SARS-CoV-2 (WIV04) or B.1.351. For the hACE2 mice challenged with

235 SARS-CoV-2 (WIV04), the PBS group showed significant loss of body weight, while

236 those animals from either mAb-treated group retained their body weight for 3 days

237 post-infection (Fig. 6a). When challenged with B.1.351, the hACE2 mice receiving

238 PBS showed gradual weight loss and reached an approximately 30% drop at day 3,

239 whereas the treatment of 58G6 or 510A5 effectively stopped the B.1.351-induced

240 weight reduction (Fig. 6a). Importantly, we found that the viral load of either

241 SARS-CoV-2 or B.1.351 in the lung tissues was significantly decreased with a single

242 dose of either mAb (Fig. 6b). These results indicate that 58G6 and 510A5 can

243 effectively protected hACE2 transgenic mice from infectious SARS-CoV-2 and

244 B.1.351, highlighting their prophylactic potential in the present COVID-19 epidemic.

245

246 **Discussion**

247 The persistence of COVID-19 has led to generation of mutational variants and

248 immunological adaptation of SARS-CoV-2[1-11]. Newly emerged B.1.351 in South

249 Africa has been reported to confer resistance to neutralization from multiple available

250 mAbs, convalescent plasma and vaccinee sera, posting a high re-infection risk[2-9]. In

251 the present study, we identified 20 neutralizing Abs with high potency against

252 authentic SARS-CoV-2 virus, from a RBD specific mAb reservoir. Among them,

253 58G6 and 510A5 exhibit high neutralizing capabilities against the authentic virus.

254 Remarkably, these 2 mAbs can efficiently neutralize authentic B.1.351 virus,

255 comparable to most effective neutralizing Abs reported up to date[2,5,6,9]. Their $IC_{50}s$

256 against this variant were as low as approximately 2 ng/mL, hence we termed these 2

257 mAbs as ultrapotent neutralizing Abs. Such profound neutralizing potencies were

258 confirmed in vivo where the prophylactic treatment of these 2 mAbs could efficiently

259 protect the transgenic mice carrying hACE2 against the airway exposure of authentic

260 SARS-CoV-2 and B.1.351 viruses. These results put 58G6 and 510A5 at the center

261 stage for the development of clinically effective therapeutic regiments against the

262 current COVID-19 pandemic.

263   In order to understand the high neutralizing potency of our mAbs against

264 SARS-CoV-2, we assessed the antigenic landscape of SARS-CoV-2 RBD. We found

265 that all our RBD targeting mAbs could be categorized into 5 groups according to their

266 recognition on the RBD. Interestingly, the epitopes recognized by the majority of our

267 potent neutralizing Abs overlapped with 13G9e, suggesting that it represented one of

268 the vulnerable sites on SARS-CoV-2 RBD. The other 4 of the top 20 mAbs competed

269 with 510A5 for the binding of RBD at 510A5e. It is worth mentioning that these 2

270 regions may correspond to 2 separate classes of epitopes recognized by the largest

271   numbers of RBD specific neutralizing Abs, as described in recent studies (Extended

272   Data Fig. 7 and 12)[18,27].

273   In detail, we identified that 58G6 recognized a region consisted of amino acids

274   450-458 in the RBD. Of note, recent cryo-EM structure analysis has revealed 3 key

275   ACE2-interacting residues (S^{Y453}, S^{L455}, and S^{F456})[13,14], indicating that $S^{450-458}$ may be

276   the critical site taken into consideration for SARS-CoV-2 prophylaxis. we found at

277   least one specific hydrogen bond within this region, between 58G6 and RBD, that

278   may contribute to recognition of the unique linear region by 58G6, rather than 13G9.

279   Although certain steric proximity of 13G9 to $S^{450-458}$ has been observed, it needs to be

280   pointed out that no specific linear binding sites have been identified for this mAb.

281   Moreover, 13G9 and 58G6 both recognized the steric epitope of $S^{470-495}$ on the

282   RBD, which was the key region shared by ACE2 and several reported potent

283   neutralizing Abs against SARS-CoV-2[13,14,22,27]. The cryo-EM analysis revealed a

284   hydrogen bond between N94 in 58G6 and the carbonyl group on the main chain,

285   rather than the side chain, of S^{E484}. Common mutation within this region found in

286   current variants, such as S^{E484K} in B.1.351 or P.1 emerged in Brazil[9,11], may not have

287   significant impact on the affinity of 58G6 to the RBDs of these variants. Indeed, the

288   sustained affinity of 58G6 to B.1.351 S1 has been confirmed by the SPR, which may

289   explain for the potentially broad neutralizing spectrum of 58G6. However, for 13G9,

290   the S^{E484K} mutation in B.1.351 or P.1 may introduce an additional positive charge

291   around R94 within its CDRL3, which may lead to strong electrostatic repulsions

292   between the two residues. This may explain the decreased affinity of 13G9 to B.1.351,

293   hence the slight decrease of neutralizing potency against this variant. As far as we

294   know, we are the first to report that an ultrapotent neutralizing Ab to SARS-CoV-2

295   with direct contact to S^{E484K} still exhibits exceptional potency against authentic

296   B.1.351 virus.

297   For the potent 13G9 or 58G6, we noted that the RBDs interacting with the 3 Fabs

298   of Abs are universally in the 'up' state. As previously described, such full occupancy

299   in each complex could render RBD completely inaccessible for ACE2[15,18,20,22].

300   However, the significance of this observed phenomena with 3-"up" conformation in

301   all particles of the Fab-S complex, in another word, its correlation to the

302   neutralization advantages, remains unknown.

303   Interestingly, we noted that 13G9 and 58G6, though originally isolated from the

304   samples of different COVID-19 convalescent donors, were both transcribed from

305   *IGHV1-58* and *IGKV3-20*. These 2 variant regions were also genetically responsible

306   for a panel of reported neutralizing Abs with high potency against SARS-CoV-2 as

307   well as B.1.351[5,6,21,22,27]. These findings highlighted the otherwise overlooked

308   importance for the pairing of the *IGHV1-58* and the *IGKV3-20* germline genes in

309   neutralizing SARS-CoV-2 and its variant.

310   In conclusion, we present 2 ultrapotent SARS-CoV-2 RBD specific mAbs with

311   exceptional efficacy against B.1.351, for which a significant proportion of reported

312   neutralizing Abs are impaired. Structural analysis of epitopes revealed the potential

313   neutralizing mechanism of neutralizing Abs against B.1.351 carrying the E484K

314   mutation. These broad-spectrum neutralizing Abs could be promising candidates for

15

315   the prophylaxis and therapeutic interventions of the pandemic of SARS-CoV-2

316   variants carrying escape mutations.

317

318   **References**

319   1.   Korber, B._, et al._ Tracking Changes in SARS-CoV-2 Spike: Evidence that
320   D614G Increases Infectivity of the COVID-19 Virus. _Cell_ **182**, 812-827.e819
321   (2020).

322   2.   Wang, P._, et al._ Antibody Resistance of SARS-CoV-2 Variants B.1.351 and
323   B.1.1.7. _Nature_ (2021).

324   3.   Wibmer, C.K._, et al._ SARS-CoV-2 501Y.V2 escapes neutralization by South
325   African COVID-19 donor plasma. _Nature Medicine_ (2021).

326   4.   Hu, J._, et al._ Emerging SARS-CoV-2 variants reduce neutralization sensitivity
327   to convalescent sera and monoclonal antibodies. _Cellular & Molecular_
328   _Immunology_ (2021).

329   5.   Chen, R.E._, et al._ Resistance of SARS-CoV-2 variants to neutralization by
330   monoclonal and serum-derived polyclonal antibodies. _Nature Medicine_
331   (2021).

332   6.   Zhou, D._, et al._ Evidence of escape of SARS-CoV-2 variant B.1.351 from
333   natural and vaccine induced sera. _Cell_ (2021).

334   7.   Planas, D._, et al._ Sensitivity of infectious SARS-CoV-2 B.1.1.7 and B.1.351
335   variants to neutralizing antibodies. _Nature Medicine_ (2021).

336   8.   Garcia-Beltran, W.F._, et al._ Multiple SARS-CoV-2 variants escape
337   neutralization by vaccine-induced humoral immunity. _Cell_,
338   S0092-8674(0021)00298-00291 (2021).

339   9.   Hoffmann, M._, et al._ SARS-CoV-2 variants B.1.351 and P.1 escape from
340   neutralizing antibodies. _Cell_ (2021).

341   10.   Tegally, H._, et al._ Sixteen novel lineages of SARS-CoV-2 in South Africa.
342   _Nature Medicine_ (2021).

343   11.   Wang, P._, et al._ Increased Resistance of SARS-CoV-2 Variant P.1 to Antibody
344   Neutralization. _bioRxiv_, 2021.2003.2001.433466 (2021).

345   12.   Li, S._, et al._ Immune characteristics analysis reveals two key inflammatory
346   factors correlated to the expressions of SARS-CoV-2 S1-specific antibodies.

17

347   *Genes & Diseases* (2020).

348   13.   Lan, J.*, et al.* Structure of the SARS-CoV-2 spike receptor-binding domain

349   bound to the ACE2 receptor. *Nature* **581**, 215-220 (2020).

350   14.   Walls, A.C.*, et al.* Structure, Function, and Antigenicity of the SARS-CoV-2

351   Spike Glycoprotein. *Cell* **181**, 281-292.e286 (2020).

352   15.   Barnes, C.O.*, et al.* Structures of Human Antibodies Bound to SARS-CoV-2

353   Spike Reveal Common Epitopes and Recurrent Features of Antibodies. *Cell*

354   **182**, 828-842.e816 (2020).

355   16.   Robbiani, D.F.*, et al.* Convergent antibody responses to SARS-CoV-2 in

356   convalescent individuals. *Nature* **584**, 437-442 (2020).

357   17.   Shi, R.*, et al.* A human neutralizing antibody targets the receptor-binding site

358   of SARS-CoV-2. *Nature* **584**, 120-124 (2020).

359   18.   Liu, L.*, et al.* Potent neutralizing antibodies against multiple epitopes on

360   SARS-CoV-2 spike. *Nature* **584**, 450-456 (2020).

361   19.   Cao, Y.*, et al.* Potent Neutralizing Antibodies against SARS-CoV-2 Identified

362   by High-Throughput Single-Cell Sequencing of Convalescent Patients' B Cells.

363   *Cell* **182**, 73-84.e16 (2020).

364   20.   Brouwer, P.J.M.*, et al.* Potent neutralizing antibodies from COVID-19 patients

365   define multiple targets of vulnerability. *Science (New York, N.Y.)* **369**, 643-650

366   (2020).

367   21.   Zost, S.J.*, et al.* Potently neutralizing and protective human antibodies against

368   SARS-CoV-2. *Nature* **584**, 443-449 (2020).

369   22.   Tortorici, M.A.*, et al.* Ultrapotent human antibodies protect against

370   SARS-CoV-2 challenge via multiple mechanisms. *Science (New York, N.Y.)*

371   **370**, 950-957 (2020).

372   23.   Wu, Y.*, et al.* A noncompeting pair of human neutralizing antibodies block

373   COVID-19 virus binding to its receptor ACE2. *Science (New York, N.Y.)* **368**,

374   1274-1278 (2020).

375   24.   Han, X.*, et al.* A Rapid and Efficient Screening System for Neutralizing

376   Antibodies and Its Application for SARS-CoV-2. *Frontiers in Immunology*

377   **12**(2021).

378 25. Wrapp, D.*, et al.* Cryo-EM structure of the 2019-nCoV spike in the prefusion

379   conformation. *Science (New York, N.Y.)* **367**, 1260-1263 (2020).

380 26. Kelley, L.A., Mezulis, S., Yates, C.M., Wass, M.N. & Sternberg, M.J.E. The

381   Phyre2 web portal for protein modeling, prediction and analysis. *Nature*

382   *Protocols* **10**, 845-858 (2015).

383 27. Dejnirattisai, W.*, et al.* The antigenic anatomy of SARS-CoV-2 receptor

384   binding domain. *Cell* (2021).

385

386 **Materials and Methods**

387 **Patient information and Isolation of antibodies to SARS-CoV-2**

388 The 74 mAbs analyzed in our manuscript were derived from a total of 39 COVID-19

389 convalescent blood samples collected within a 2-month window post discharge. These

390 39 convalescent patients have an average age of 45 years old, and majority of them

391 exhibited mild symptoms, as described in the previous study[24]. The original studies to

392 obtain blood samples after written informed consent were previously described and

393 had been approved by the Ethics Board of ChongQing Medical University[24]. Briefly,

394 we utilized SARS-CoV-2 RBD as bait to sort the antigen-specific memory B cells

395 from the COVID-19 convalescent patients. The IgG heavy and light chains of mAbs

396 genes in these memory B cells were obtained by single cell PCR and transiently

397 transfected into HEK293T cells for the identification of mAbs with capabilities of the

398 neutralization against SARS-CoV-2 pseudovirus. With such rapid screening system,

399   we were capable to obtain the defined neutralizing Abs within 6 days.

400   **Recombinant antibody production and purification**

401   A pair of plasmids separately expressing the heavy- and the light- chain of antibodies

402   were transiently co-transfected into Expi293™ cells (Catalog No. A14528,

403   ThermoFisher) with ExpiFectamine™ 293 Reagent. Then the cells were cultured in

404   shaker incubator at 120 rpm and 8% CO_2 at 37℃. After 7 days, the supernatants with

405   the secretion of antibodies were collected and captured by protein G Sepharose (GE

406   Healthcare). The bound antibodies on the Sepharose were eluted and dialyzed into

407   phosphate-buffered saline (PBS). The purified antibodies were used in following

408   binding and neutralization analyses.

409   **Authentic SARS-CoV-2 neutralization assay**

410   The neutralizing potency of mAbs against authentic SARS-CoV-2 virus quantified via

411   qRT-PCR was performed in a biosafety level 3 laboratory of Fudan University.

412   Serially diluted mAbs or mAbs mixture (1:1 with same quality) were incubated with

413   authentic SARS-CoV-2 virus (nCoV-SH01, GenBank: MT121215.1, 100 TCID50) for

414   1 h at 37 °C. After the incubation, the mixtures were then transferred into 96-well

415   plates, which were seeded with Vero E6 cells. The plates were kept at 37 °C for 48 hrs.

416   And the supernatant viral RNA load of each well was quantified by qRT-PCR. For

417   qRT-PCR, the viral RNA was extracted from the collected supernatant using Trizol LS

418   (Invitrogen) and used as templates for the qRT-PCR analysis by Verso 1-Step

419   qRT-PCR Kit (Thermo Scientific) following the manufacturer's instructions. PCR

420   primers targeting SARS-CoV-2 N gene (nt 608-706) were as followed, forward:

421 5'-GGGGAACTTCTCCTGCTAGAAT-3', and reverse:

422 5'-CAGACATTTTGCTCTCAAGCTG-3'. qRT-PCR was performed using the

423 LightCycler 480 II PCR System (Roche) with the following program: 50 °C 15 mins;

424 95 °C 15 mins; 40 cycles of 95 °C 15 seconds, 50 °C 30 seconds, 72 °C 30 seconds.

425 The IC_{50} and IC_{80} of the evaluated mAbs was and calculated by a four-parameter

426 logistic regression using GraphPad Prism 8.0.

427 The neutralizing potency of mAbs against authentic SARS-CoV-2 and B.1.351

428 viruses was performed quantified via PRNT in a biosafety level 3 laboratory of

429 Wuhan Institute of Virology. Each mAb sample was serially diluted with DMEM as

430 two folds and the sample quality, mixed with equal volume of authentic SARS-CoV-2

431 virus (WIV04, GenBank: MN996528.1) or SARS-CoV-2 South Africa strain B.1.351

432 (NPRC 2.062100001, GenBank: MW789246.1) and incubated at 37 °C for 1 h. Vero

433 E6 cells in 24-well plates were inoculated with the sera-virus mixture at 37 °C; 1 h.

434 Later, the mixture was replaced with DMEM containing 2.5% FBS and 0.8%

435 carboxymethylcellulose. The plates were fixed with 8% paraformaldehyde and stained

436 with 0.5% crystal violet 4 days later. All samples were tested in duplicate and

437 neutralization titers were defined as the serum dilution resulting in a plaque reduction

438 of at least 50%[30].

439 **Sequence analysis of antigen-specific mAbs**

440 IMGT/V-QUEST (http://www.imgt.org/ IMGT_vquest /vquest) and IgBLAST

441 (https://www.ncbi.nlm.nih.gov/igblast/), MIXCR (https://mixcr.r

442 eadthedocs.io/en/master/) and VDJtools

21

443 (https://vdjtools-doc.readthedocs.io/en/master/overlap.html) tools were used to do the

444 variable region analysis and annotation for each antibody clone.

Production of pseudovirus bearing S protein

446 pVSVG expressing SARS-CoV-2 S protein was constructed as previously described[29].

447 The packaging plasmid (VSV-G pseudotyped ΔG-luciferase) encoding either the S

448 protein of SARS-CoV-2, B.1.1.7 or chimeric construct including B.1.351 RBD and

449 S^{D614G} was generated. HEK293T cells were grown to 80% confluency before

450 transfection with VSV-G pseudotyped ΔG-luciferase, pWPXL and pSPAX2. These

451 cells were cultured overnight at 37 °C with 5% CO_2. DMEM supplemented with 5%

452 fetal bovine serum and 100 IU/mL of penicillin and 100 μg/mL of streptomycin was

453 added to the inoculated cells, which were cultured overnight for 72 hrs. The

454 supernatant was harvested, filtered by 0.45 μm filter and centrifugated at 300 g for 10

455 mins to collect the supernatant, then aliquoted and storied at -80 °C.

Pseudovirus neutralization assay

457 Serially diluted mAbs with volume of 50 μL were incubated with the same volume of

458 the HEK293T cell supernatants containing the pseudovirus for 1 h at 37 °C. These

459 pseudovirus-antibody mixtures were added to ACE2 expressing HEK293T cells

460 (HEK293T/ACE2). After 72 hrs, the luciferase activities of infected HEK293T/ACE2

461 cells were detected by the Bright-Luciferase Reporter Assay System (Promega,

462 E2650). The IC_{50} of the evaluated mAbs was tested by the Varioskan LUX Microplate

463 Spectrophotometer (Thermo Fisher), and calculated by a four-parameter logistic

464 regression using GraphPad Prism 8.0.

22

465 **Protein expression and purification**

466 To express the prefusion S ectodomain, the gene encoding residues 1-1208 of

467 SARS-CoV-2 S (GenBank: MN908947.3) with a C-terminal T4 fibritin trimerization

468 motif, an HRV-3C protease cleavage site, a Twin-Strep-tag and an $8 \times$ His-tag was

469 synthesized, and cloned into the mammalian expression vector pcDNA3.1, which was

470 a kind gift from L. Sun at Fudan University, China. The gene of the S protein was

471 constructed with proline substitutions at residues 986 and 987, a "GSAS" instead of

472 "RRAR" at the furin cleavage site (residues 682-685) according to Jason S.

473 McLellan's research[25].

474　Expi293 cells (Thermo Fisher Scientific, USA) cultured in Freestyle 293

475 Expression Medium (Thermo Fisher Scientific, USA) were maintained at 37 °C. Cells

476 were diluted to a density of 2.5×10^6 to 3×10^6 cells per mL before transfection. For

477 protein production, 1.2 mg DNA was mixed with 3 mg polyethyleneimine in 30 mL

478 Freestyle 293 Expression Medium, incubated for 20 mins, then added to 1000 mL of

479 cells[31]. Transfected cells were cultured at 35 °C, and the cell culture supernatant was

480 collected at day 4 to day 5.

481 The protein was purified from filtered cell supernatants using Strep-Tactin resin (IBA)

482 before being subjected to additional purification by gel filtration chromatography

483 using a Superose 6 10/300 column (GE Healthcare, USA) in $1 \times$ PBS, pH 7.4

484 (Extended Data Fig. 10a, b).

485 **Cryo-EM sample preparation and data collection**

486 Purified SARS-CoV-2 S was diluted to a concentration of 1.5 mg/mL in PBS, pH 7.4.

23

487   5 μL of purified SARS-CoV-2 S was mixed with 1 μL of 58G6 Fab fragments at 2

488   mg/mL in PBS and incubated for 30 mins on ice. A 3 μL aliquot of the mixture (added

489   with 0.01% DDM) was applied onto an H_2/O_2 glow-discharged, 300-mesh Quantifoil

490   R1.2/1.3 grid (Quantifoil, Micro Tools GmbH, Germany). The grid was then blotted

491   for 3.0 s with a blot force of -1 at 8 °C and 100% humidity and plunge-frozen in

492   liquid ethane using a Vitrobot (Thermo Fisher Scientific, USA). Cryo-EM data sets

493   were collected at a 300 kV Titan Krios microscope (Thermo Fisher Scientific, USA)

494   equipped with a K3 detector (Gatan, USA). The exposure time was set to 2.4 s with a

495   total accumulated dose of 60 electrons per $Å^2$, which yields a final pixel size of 0.82

496   Å. 2605 micrographs were collected in a single session with a defocus range

497   comprised between 1.0 and 2.8 μm using SerialEM. The sample preparation and data

498   collection for the SARS-CoV-2 S-13G9 Fab complex were in accordance with the

499   SARS-CoV-2 S-58G6 Fab complex. The statistics of cryo-EM data collection can be

500   found in Extended Data Table 1.

501   **Cryo-EM data processing**

502   All dose-fractioned images were motion-corrected and dose-weighted by

503   MotionCorr2 software[32] and their contrast transfer functions were estimated by

504   cryoSPARC patch CTF estimation[33]. For the dataset of SARS-CoV-2 S-58G6 Fab

505   complex, a total of 1,255,599 particles were auto-picked using the template picker and

506   820,872 raw particles were extracted with a box size of 512 pixels in cryoSPARC[33].

507   The following 2D, 3D classifications, and refinements were all performed in

508   cryoSPARC. 237,062 particles were selected after two rounds of 2D classification,

24

509 and these particles were used to do Ab-Initio reconstruction in six classes. Then these

510 six classes were used as 3D volume templates for heterogeneous refinement with all

511 selected particles, with 108,020 particles converged into the SARS-CoV-2 S-58G6

512 Fab class. Next, this particle set was used to perform non-uniform refinement,

513 yielding a resolution of 3.56 Å.

514 For the dataset of SARS-CoV-2 S-13G9 Fab complex, a total of 445,137 particles

515 were auto-picked using the template picker and 266,357 raw particles were extracted

516 with a box size of 512 pixels in cryoSPARC. The following 2D, 3D classifications,

517 and refinements were all performed in room temperature (RT). 70,519 particles were

518 selected after two rounds of 2D classification, and these particles were used to do

519 Ab-Initio reconstruction in six classes. Then these 6 classes were used as 3D volume

520 templates for heterogeneous refinement with all selected particles, with 52,880

521 particles converged into the SARS-CoV-2 S-13G9 Fab class. Next, this particle set

522 was used to perform non-uniform refinement, yielding a resolution of 3.92 Å.

523 Although the overall resolution for these structures is up to 3.5 Å - 3.6 Å for 58G6

524 and 3.9 Å - 4.0 Å for 13G9, the maps for the binding interface between RBD and Fabs

525 are quite weak due to the conformational heterogeneity of the RBD, which is similar

526 to previous structural investigations[15,18,22,34]. To improve the resolution for the binding

527 interface, we subsequently added local refinement processing. A local reconstruction

528 focusing on the RBD-Fabs region was carried out. Furthermore, the density map for

529 the binding interface could be improved further by local averaging of the RBD-Fab

530 equivalent copies, finally yielding a 3.5 Å map of the region corresponding to the

531   58G6 variable domains and the RBD (Extended Data Fig. 10c, f). Similarly, we

532   improve the local resolution between the 13G9 variable domains and the RBD up to

533   3.8 Å (Extended Fata Fig. 10g, j).

534   Local resolution estimation, filtering, and sharpening were also carried out using

535   cryoSPARC. The full cryo-EM data processing workflow is described in Extended

536   Data Fig. 10 and the model refinement statistics can be found in Extended Data Table

537   1.

538   **Model Building and Refinement**

539   To build the structures of the SARS-CoV-2 S-58G6 Fab and S-13G9 Fab complexes,

540   the structure of the SARS-CoV-2 S glycoprotein in complex with the C105

541   neutralizing antibody Fab fragment[15] (PDB: 6XCN) was placed and rigid-body fitted

542   into the cryo-EM electron density maps using UCSF Chimera[35], respectively. Both of

543   the 58G6 and 13G9 Fab models were first predicted using Phyre2[26] and then manually

544   built in Coot 0.9[36] with the guidance of the cryo-EM electron density maps, and

545   overall real-space refinements were performed using Phenix 1.18[37]. The data

546   validation statistics are shown in Extended Data Table 1.

547   **Creation of Figures**

548   Figures of molecular structures were generated using PyMOL[38] and UCSF

549   ChimeraX[39].

550   **The antibody binding kinetics and the competition with ACE2 measured by SPR**

551   The affinity of the neutralizing Abs binding to the S1 subunit of SARS-CoV-2 or

552   B.1.351 was measured using the Biacore X100 platform at RT. A CM5 chip (GE

26

553   Healthcare) was linked with anti-human IgG-Fc antibody to capture about 9000

554   response units of the neutralizing Abs. The gradient concentrations of SARS-CoV-2

555   S1 or an artificial chimeric construct carrying 3 mutations on B.1.351 RBD and S^{D614G}

556   (B.1.351 S1) (Sino Biological, Beijing, China) were prepared (2-fold dilutions, from

557   50 nM to 0.78 nM) with HBS-EP$^+$ Buffer (0.01 M HEPES, 0.15 M NaCl, 0.003 M

558   EDTA and 0.05% (v/v) Surfactant P20, pH 7.4), and sequentially injected into the

559   chip and monitored for the binding kinetics. After the final reading, the sensor surface

560   of the chip was regenerated with 3 M $MgCl_2$ (GE) before the measurement of the next

561   mAb. The affinity was calculated with Biacore X100 Evaluation Software

562   (Version:2.0.2) using 1:1 binding fit model.

563   To determine competition with the ACE2 peptidase domain, SARS-CoV-2 RBD

564   was coated on a CM5 sensor chip via amine group for a final RU around 250. The top

565   20 neutralizing Abs (20 μg/mL) were injected onto the chip until binding steady-state

566   was reached. ACE2 (20 μg/mL) was then injected for 60 seconds. Blocking efficacy

567   was determined by comparison of response units with and without prior antibody

568   incubation.

569   **Competitive ELISA**

570   For competitive ELISA used in epitope mapping of mAbs, 2 μg/mL recombinant

571   RBD-his (Sino Biological, Beijing, China) was added in 384-well plates and

572   incubated at 4 °C overnight. 50 μg/mL mAbs per well were added. The plates were

573   incubated at 37 °C for 1 h and then washed. Biotinylation of mAbs (the top 20

574   neutralizing Abs and 81A11, previously reported SARS-CoV CR3022[28]) was

27

575   performed using the EZ-link NHS-PEO Solid Phase Biotinylation Kit (Pierce)

576   according to the manufacturer's protocol and purified using MINI Dialysis Unit

577   (ThermoFisher, 69576). 500 ng/mL biotinylated mAbs were added to each well, and

578   the plates were incubated at 37 °C for 1 h. ALP-conjugated streptavidin (Mabtech,

579   Sweden, 3310-10) was added at 1:1000, followed by an incubation of 30 mins at

580   37 °C. For the quantification of bound IgG, PNPP (Thermo Fisher) was added at 1

581   mg/mL and the absorbance at 405 nm was measured by the MultiSkan GO

582   fluoro-microplate reader (Thermo Fisher).

583   **Western blot analysis**

584   The recombinant RBD protein was mixed with $5 \times$ loading buffer (Beyotime,

585   Shanghai, China) and denatured for 5 mins at 100 °C. The denatured proteins (200 ng)

586   were subjected to electrophoresis with 10% SDS-polyacrylamide gel and then

587   transferred to PVDF membranes. After blocking by skim milk (Biofroxx), the

588   membranes were incubated at 4 °C overnight, with the purified mAbs as primary Abs.

589   The next days, the membranes were washed with TBST and incubated with

590   HRP-conjugated Goat-anti-human Fc antibody (Abcam, ab99759, 1:10000) for 1 h at

591   RT. The membranes were examined on ChemiDoc Imaging System (Bio-rad).

592   **Peptide ELISA**

593   Peptide ELISA was performed with synthesized peptides overlapping with 5 amino

594   acids (Genescripts, Wuhan, China). These peptides were tethered by N-terminal

595   biotinylated linker peptides (biotin-ahx), except for the first peptide at the N-terminus,

596   whose biotin was linked to the C terminus instead. The RBD9-1 amino acid residues

28

597   were selected and mutated to alanine and synthesized by Genescripts (Wuhan, China).

598   50 μL synthesized peptide was added to the streptavidin-coated 384-well plate in

599   duplets to make a final concentration of 5 μg/mL. The plates were incubated for 2 hrs

600   at RT. After washing, the plates were blocked with Protein-Free Blocking Buffer

601   (Pierce, USA, 37573) at RT for 1 h and incubated with 10 μg/mL testing mAbs at RT

602   for another 1 h. Reacted mAbs were detected using ALP-conjugated Goat F(ab')$_2$

603   Anti-Human IgG (Fab')$_2$ secondary antibody conjugated with ALP (Abcam, ab98532,

604   1:2000) for 30 mins at RT, followed with quantification detection.

605   For the ACE2 competitive peptide ELISA, 5 μg/mL synthesized RBD9-1 was

606   immobilized on the streptavidin-coated 384-well plate at RT for 2 hrs. After washing

607   with Protein-Free Blocking Buffer, the plates were blocked with this blocking buffer.

608   Next, serial diluted 58G6 (20-0.625 μg/mL) in 50 μL of the blocking buffer were

609   added into plate and the plates were incubated at RT for 1 h. Then, the plate incubated

610   with 2 μg/mL ACE2 at RT for another 1 h. The ELISA plates were washed 4 times by

611   blocking buffer and 50 μL Goat F(ab')$_2$ Anti-Human IgG (Fab')$_2$ secondary antibody

612   conjugated with ALP (Abcam, ab98532, 1:2000) was incubated with the plate at RT

613   for 30 mins. The plate was washed and followed with quantification detection.

614   **Authentic SARS-CoV-2 and B.1.351 viruses and animal study**

615   Authentic SARS-CoV-2 (WIV04) and B.1.351 (NPRC 2.062100001) viruses were

616   propagated on the Vero-E6 cells and titrated by single layer plaque assay with

617   standard procedure. The hACE2 mouse model was used to evaluate the efficacy of

618   58G6 and 510A5 monoclonal antibodies *in vivo*. Six- to eight-week-old female

29

619 hACE2 mice were treated with 58G6 or 510A5 monoclonal antibody at a

620 concentration of 10 mg/kg by intraperitoneal route, respectively. The mice treated

621 with PBS were used as the negative control. 24 hours later, all mice were intranasally

622 infected with 10^5 PFU authentic SARS-CoV-2 or B.1.351 viruses in a total volume of

623 50 μL. At 3 days post infection of SARS-CoV-2 or B.1.351, the lungs of mice were

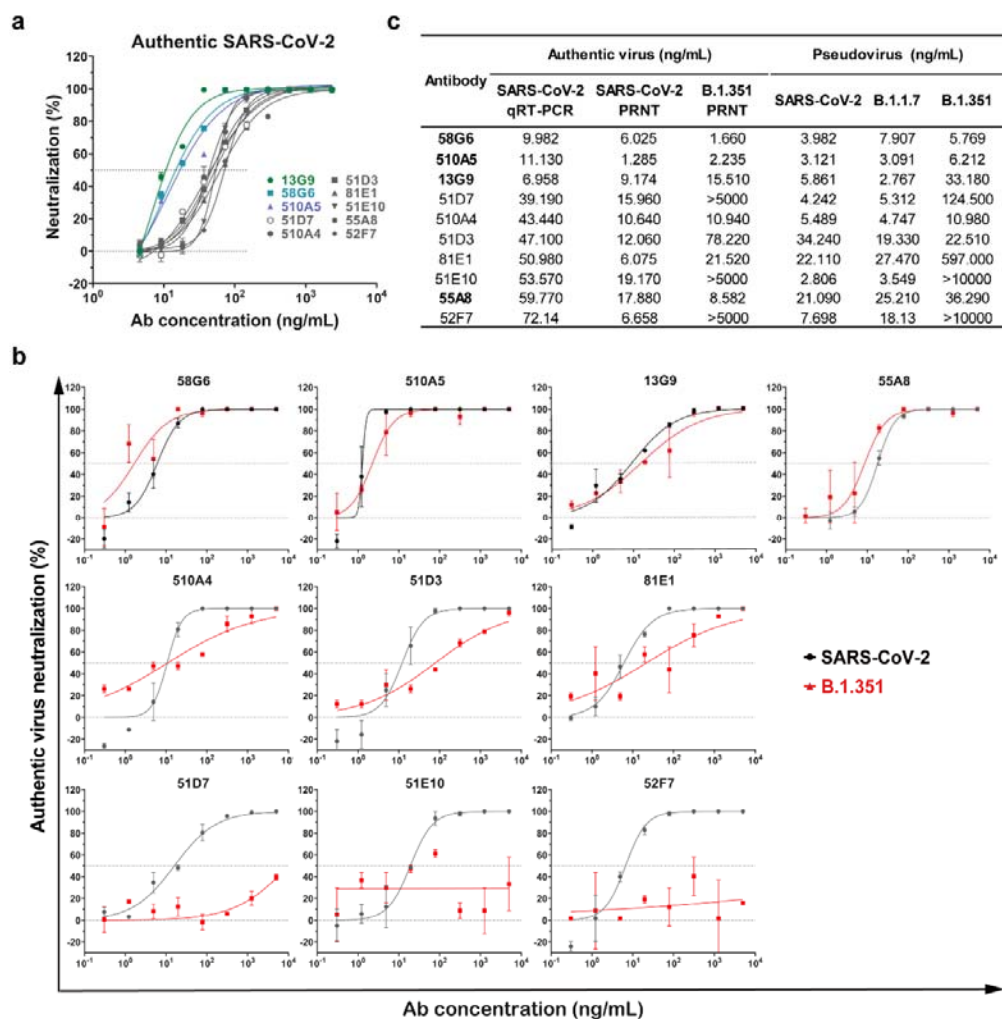624 collected for viral load determination using plaque assay[40].

Data analysis

626 Data are shown as mean ± SEM. Two-group comparisons were performed by

627 Student's t-test. The difference was considered significant if $p < 0.05$.

628 **References**

629 28. Meulen, J., *et al.* Human monoclonal antibody combination against SARS

630 coronavirus: synergy and coverage of escape mutants. *PLoS medicine* **3**, e237

631 (2006).

632 29. Ou, X., *et al.* Characterization of spike glycoprotein of SARS-CoV-2 on virus

633 entry and its immune cross-reactivity with SARS-CoV. *Nature*

634 *Communications* **11**, 1620 (2020).

635 30. Singh, K., *et al.* The Vaccinia Virus H3 Envelope Protein, a Major Target of

636 Neutralizing Antibodies, Exhibits a Glycosyltransferase Fold and Binds

637 UDP-Glucose. *Journal of Virology*, 5020 (2016).

638 31. Xiong, X., *et al.* A thermostable, closed SARS-CoV-2 spike protein trimer.

639 *Nature Structural & Molecular Biology* (2020).

640 32. Zheng, S.Q., *et al.* MotionCor2: anisotropic correction of beam-induced

641 motion for improved cryo-electron microscopy. *Nature Methods* **14**, 331-332

642 (2017).

643 33. Punjani, A., Rubinstein, J.L., Fleet, D.J. & Brubaker, M.A. cryoSPARC:

644 algorithms for rapid unsupervised cryo-EM structure determination. *Nature*

645   *Methods* **14**, 290-296 (2017).

646   34.   Barnes, C.O.*, et al.* SARS-CoV-2 neutralizing antibody structures inform
647   therapeutic strategies. *Nature* **588**, 682-687 (2020).

648   35.   Pettersen, E.F.*, et al.* UCSF Chimera-A visualization system for exploratory
649   research and analysis. *Journal of Computational Chemistry* **25**, 1605-1612
650   (2004).

651   36.   Emsley, P., Lohkamp, B., Scott, W.G. & Cowtan, K. Features and development
652   of Coot. *Acta Crystallographica Section D* **66**, 486-501 (2010).

653   37.   Liebschner, D.*, et al.* Macromolecular structure determination using X-rays,
654   neutrons and electrons: recent developments in Phenix. *Acta
655   Crystallographica Section D* **75**, 861-877 (2019).

656   38.   Schrodinger, LLC. The PyMOL Molecular Graphics System, Version 1.8.
657   (2015).

658   39.   Goddard, T.D.*, et al.* UCSF ChimeraX: Meeting modern challenges in
659   visualization and analysis. *Protein Science* **27**, 14-25 (2018).

660   40.   Zhang, Y.N.*, et al.* A mouse model for SARS-CoV-2 infection by exogenous
661   delivery of hACE2 using alphavirus replicon particles. *Cell Res* **30**, 1046-1048
662   (2020).

663

664   **Figures and Tables**

Antibody	Authentic virus (ng/mL)			Pseudovirus (ng/mL)		
	SARS-CoV-2 qRT-PCR	SARS-CoV-2 PRNT	B.1.351 PRNT	SARS-CoV-2	B.1.1.7	B.1.351
58G6	9.982	6.025	1.660	3.982	7.907	5.769
510A5	11.130	1.285	2.235	3.121	3.091	6.212
13G9	6.958	9.174	15.510	5.861	2.767	33.180
51D7	39.190	15.960	>5000	4.242	5.312	124.500
510A4	43.440	10.640	10.940	5.489	4.747	10.980
51D3	47.100	12.060	78.220	34.240	19.330	22.510
81E1	50.980	6.075	21.520	22.110	27.470	597.000
51E10	53.570	19.170	>5000	2.806	3.549	>10000
55A8	59.770	17.880	8.582	21.090	25.210	36.290
52F7	72.14	6.658	>5000	7.698	18.13	>10000

665

666   **Fig. 1 | The neutralizing capabilities of the top 10 mAbs against authentic**

667   **SARS-CoV-2 and B.1.351 viruses.** The neutralizing potency of the top 10 mAbs was

668   measured by authentic SARS-CoV-2 (nCoV-SH01) neutralization assay and

669   quantified by qRT-PCR (a) or authentic SARS-CoV-2 (WIV04) and B.1.351

670   neutralization assays and quantified by PRNT (b). The IC_{50}s were summarized in (c).

671   Dashed line indicated 0% or 50% reduction in viral neutralization. Data for each mAb

672   were obtained from a representative neutralization experiment, with at least two

32

673   replicates, presented as mean ± SEM. Effective Abs against authentic B.1.351 were

674   shown in bold.

675

33
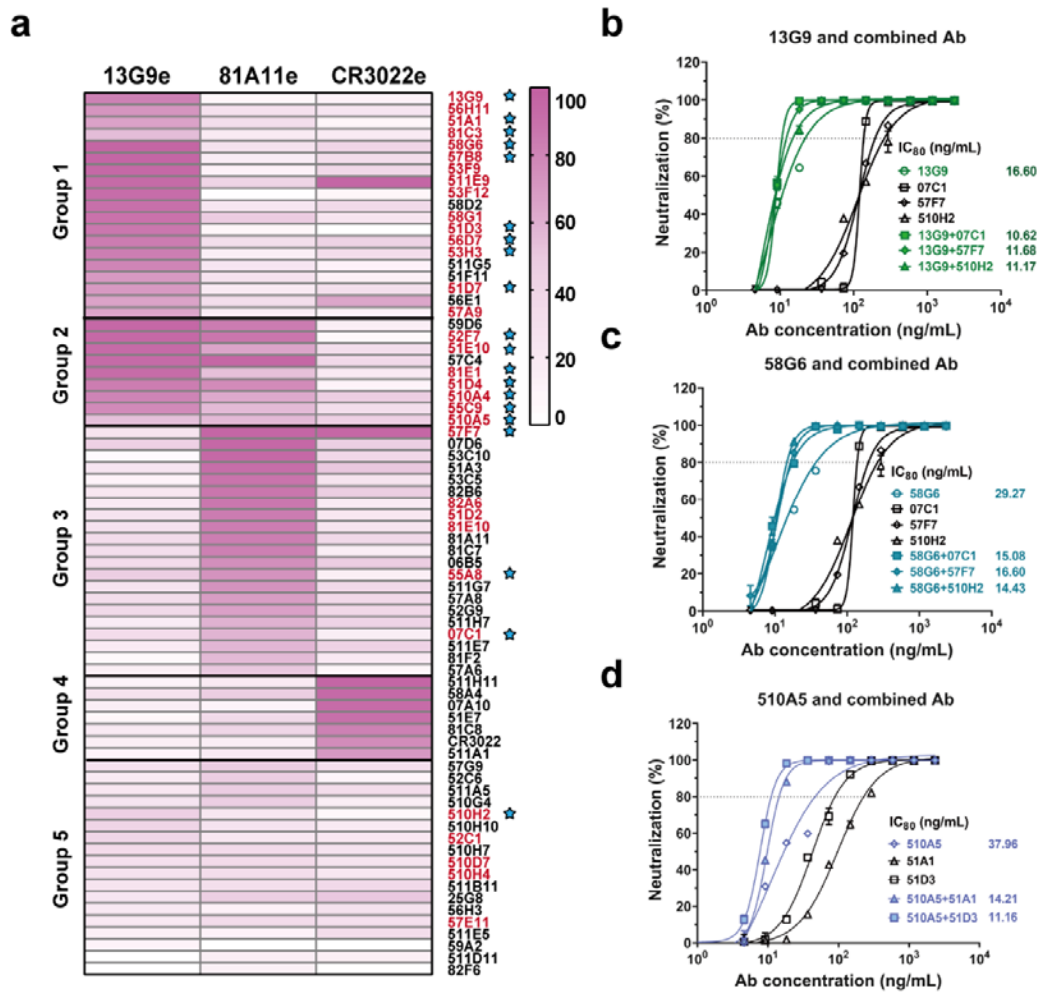
676

677 **Fig. 2 | Epitope mapping of mAbs and the analysis of neutralizing Abs from**

678 **different groups.** (a) Epitope mapping of purified mAbs targeting three independent

679 epitopes (13G9e, 81A11e and CR3022e). All mAbs in Group 1 competed with 13G9;

680 each mAb in Group 3 competed with 81A11; Group 2 consisted of mAbs

681 cross-reacted with 13G9e and 81A11e, the latter to a lesser extent; all mAbs in Group

682 4 targeted the epitopes overlapping with CR3022e, and the mAbs in Group 5

683 recognized none of these 3 epitopes. All neutralizing Abs identified by authentic

684 SARS-CoV-2 CPE assay were labelled in red. The top 20 mAbs identified by

685 qRT-PCR with authentic SARS-CoV-2 virus were indicated by blue stars. The

34

686   synergistic effects of 13G9 (b) and 58G6 (c) with 07C1 or 57F7 recognizing 81A11e,

687   or 510H2 with no clearly identified epitope, against authentic SARS-CoV-2 virus

688   were quantified by qRT-PCR. (d) The synergistic effects of 510A5 with 51A1 or

689   51D3 recognizing 13G9e, against authentic SARS-CoV-2 virus were quantified by

690   qRT-PCR. Dashed line indicated 80% inhibition in the viral infectivity. Data for each

691   mAb were obtained from a representative neutralization experiment of three replicates,

692   presented as mean ± SEM.

693
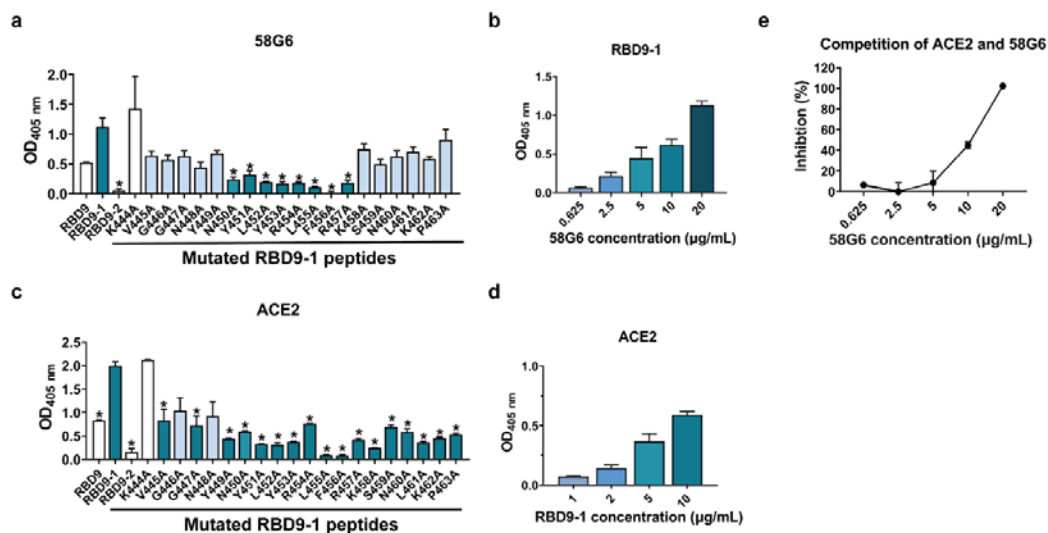
Fig 3. | The interaction of 58G6 with a linear region in the denatured RBD.

ELISA results of the binding activities of 58G6 (a) or ACE2 (c) to 3 peptides covering sequences in close proximity, RBD9, RBD9-1 and RBD9-2, and single mutations derived from the full length RDB9-1. The binding activity of 58G6 (b) or ACE2 (d) in various concentrations to the RBD9-1 peptide, tested by ELISA. (e) The ability of 58G6 in blocking the interaction between RBD9-1 and ACE2, tested by competitive ELISA. Data are representative of at least 2 independent experiments performed in technical duplicate. The mean ± SEM of duplicates are shown. *, $p < 0.05$.

704
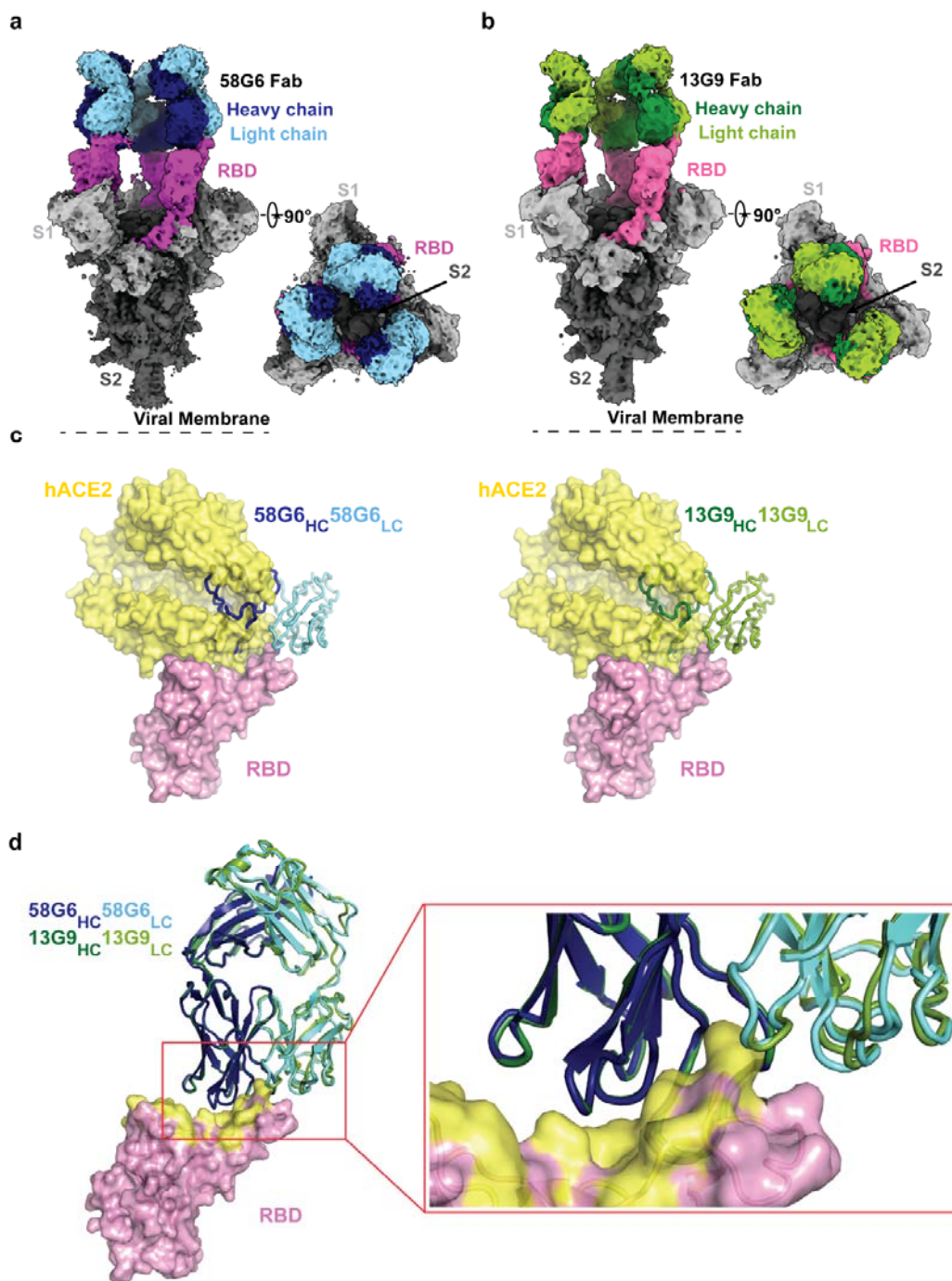
Fig. 4 | Cryo-EM structures of 58G6 and 13G9 Fabs binding to open S trimer. (a,

b) Cryo-EM densities for 58G6 Fab-S (a; 3.6 Å) and 13G9 Fab-S (b; 3.9 Å)

complexes, revealing binding of 58G6 or 13G9 to RBDs in the all 'up' state. (c)

Superimposition of RBD-hACE2 [Protein Data Bank (PDB) ID 6LZG] complex

709   structure together with RBD-58G6 Fab (left) or RBD-13G9 Fab (right) variable

710   domains, respectively. (d) Alignment of 58G6 and 13G9 Fabs on the same RBD. HC,

711   heavy chain; LC, light chain.

712
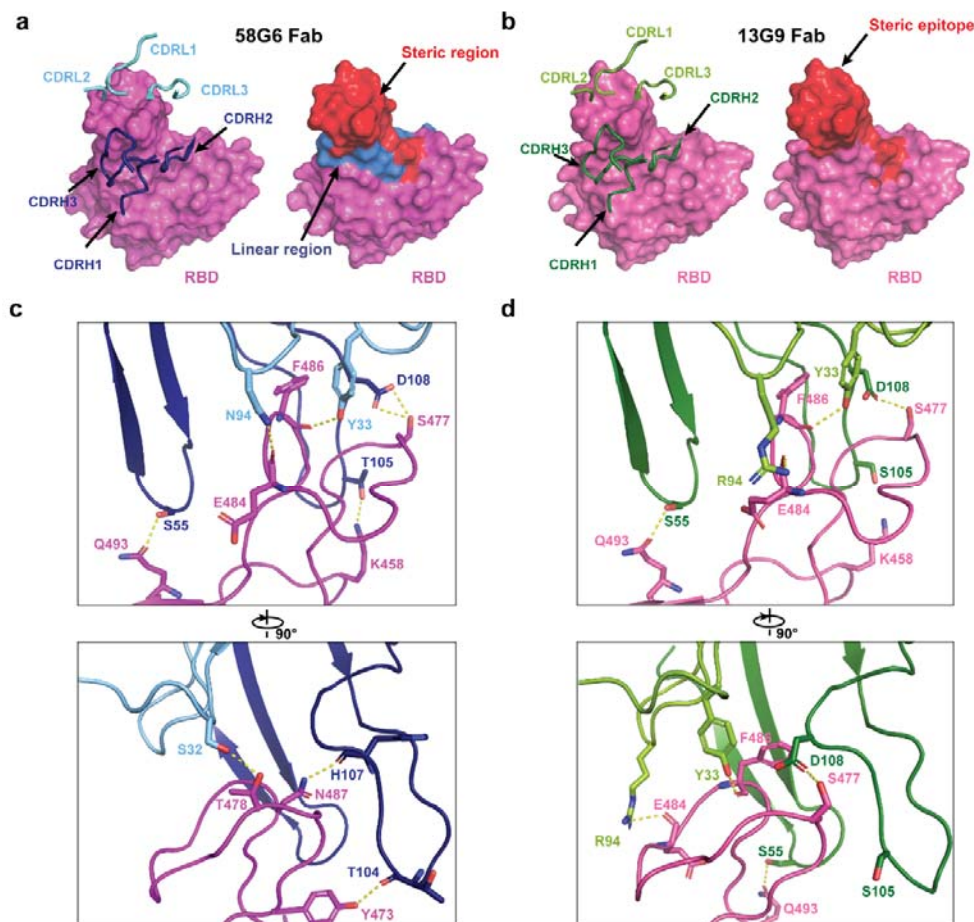
Fig. 5 | Details of interactions between SARS-CoV-2 RBD and mAbs. (a, b) CDR loops of 58G6 Fab (a, left) and 13G9 Fab (b, left) overlaid on the surface representation of RBD (shown as pink and magenta, respectively), and surface representations of 58G6 epitope (a, right, red and blue) and 13G9 epitope (b, right, red) on the RBD surface. (c, d) The hydrogen bonds at the binding interface between 58G6 (left) or 13G9 (right) and SARS-CoV-2 RBD.

719

39
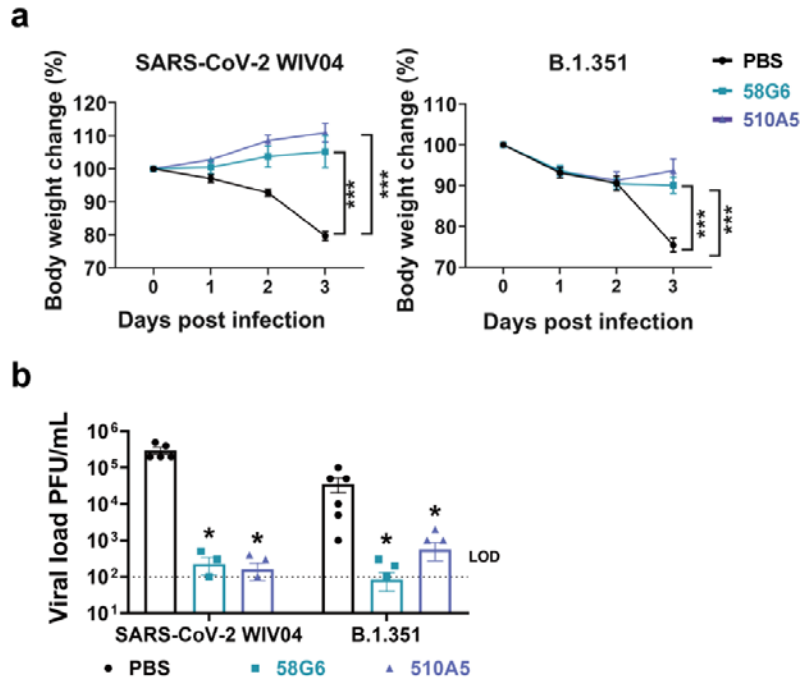
Fig. 6 | The prophylactic efficacy of 58G6 or 510A5 in hACE2 transgenic mice challenged with authentic viruses. (a) Body weight changes were recorded for PBS (SARS-CoV-2 (WIV04): n = 5; B.1.351: n = 6), 58G6 (SARS-CoV-2 (WIV04): n = 4; B.1.351: n = 7) and 510A5 (SARS-CoV-2 (WIV04): n = 5; B.1.351: n = 7) treatment groups. All the mice received one dose of antibodies (10 mg/kg body weight) injected (i.p.) 24 hours prior to the intranasal challenge with SARS-CoV-2 (WIV04) (left) or B.1.351 (right). Equal volume of PBS was used as negative control. The weight loss was recorded over 3 days. (b) The virus loads in infected lungs were determined by PRNT at 3 days post infection (dpi). $*p < 0.1$, $***p < 0.001$.

732

Data availability

733

The coordinates and structure factor files for the 13G9/SARS-CoV-2 RBD complex

734

and 58G6/SARS-CoV-2 RBD complex have been deposited in the Protein Data Bank

735

(PDB) under accession number 7E3K and 7E3L respectively.

736

Author contributions

748

A.J. and A.H. conceived and designed the study. F.L. and H.J. were responsible for

749

antibody production and purification. J.W., K.W., J.H., S.L., N.T., G.Z. and Q.G.

750

conducted the pseudovirus neutralization assays and Y.X., C.G., Y.W., W.X., X.C.,

751

D.Q. and Z.Y. performed authentic SARS-CoV-2 neutralization assays. S.L. and Y.H.

752

played an import role in data analysis of neutralizing Abs sequences. T.L., Y.W., Y.L.,

753

754   S.S., Q.C., F.G. and M.S. performed ELISA, competitive ELISA and peptide ELISA.

755   X.H., C.H., R.W. and S.M. were responsible for SPR assay for the affinity of these

756   neutralizing Abs and competition of these neutralizing Abs with ACE2. H.G., F.L.,

757   Y.G., W.W., X.J. and H.Y. carried out the cryo-EM studies. H.Z, Y.Z, Z.Z, H.Z, N.L

758   and B.Z were responsible for the prophylactic test of neutralizing Abs for hACE2

759   mice challenged with SARS-CoV-2 and B.1.351. L.L. and C.H. generated figures and

760   tables, and take responsibility for the integrity and accuracy of the data presentation.

761   A.J., T.L., W.W. and H.G wrote the manuscript.

762   **Declaration of Interests**

763   Patent has been filed for some of the antibodies presented here.

764   **Ethics statement**

765   The project "The application of antibody tests patients infected with SARS-CoV-2"

766   was approved by the ethics committee of Chongqing Medical University. Informed

767   consents were obtained from all participants.

768   All the mice were cared in accordance with the recommendations of National

769   Institutes of Health Guidelines for the Care and Use of Experimental Animals. Viral

770   infections were conducted in an animal biosafety level 3 (ABSL-3) facility at Wuhan

771   Institute of Virology under a protocol approved by the Laboratory Animal Ethics

772   Committee of Wuhan Institute of Virology, Chinese Academy of Sciences (Permit

773   number: WIVA26201701).